*J. Fluid Mech.* (2006), *vol.* 555, *pp.* 141–148.  
doi:10.1017/S0022112006009220 Printed in the United Kingdom

# On the resonance of a pliant tube as a mechanism for valveless pumping

By A. I. HICKERSON† AND M. GHARIB

Option of Bioengineering, California Institute of Technology,
1200 E California Blvd., Pasadena, CA 91125, USA

(Received 4 October 2005 and in revised form 29 January 2006)

Valveless pumping can be achieved through the periodic compression of a pliant tube asymmetrically from its interfaces to different tubing or reservoirs. A mismatch of characteristic impedance between the flow channels is necessary for creating wave reflection sites. Previous experimental studies of the behaviour of such a pump were continued in order to demonstrate the wave mechanics necessary for the build-up of pressure and net flow. Specific measurements of the transient and resonant properties were used to relate the bulk responses to the pump mechanics. Ultrasound imaging through the tube wall allowed visualization of the wall motion concurrently with pressure and flow measurements. For analysis, a one-dimensional wave model was constructed which predicted many of the characteristics exhibited by the experiments.

## 1. Introduction

Valveless pumping can be achieved by periodically compressing a pliant tube at an asymmetric location from rigid ends. The compression will produce a frequency-dependent net flow. This phenomenon was first discovered by Liebau (1954). In the ensuing years, analytical and computational studies have been presented to model possible mechanics responsible for this phenomenon. These models were derived from first principles of solid and fluid mechanics (Thomann 1978; Mahrenholtz 1963; Moser *et al.* 1998; Kenner *et al.* 2000; Jung & Peskin 2001; Borzi & Propst 2003; Ottesen 2003; Auerbach, Moehring & Moser 2004). Comprehensive experimental results on the bulk flow behaviours were collected by Hickerson, Rinderknecht & Gharib (2005). These results showed that the direction of flow is dependent on the frequency of compression. The net pressure head and net flow as a function of the compression frequency had distinct peaks at selected frequencies.

Concurrent with the pumping studies, additional research analysed the forced flow through elastic vessels by means of applying a pressure gradient across the ends. Bertram, Raymond & Pedley (1991), among others, have demonstrated that for certain conditions the vessel will flutter due to a resonance in the tube. This inspired the notion that the problem of modelling the pumping phenomenon can be approached as the reverse process of tube fluttering. Further experimentation, as a continuation of the work of Hickerson *et al.* (2005), was necessary to qualify the resonant behaviours observed. A predictive model could then be constructed to determine the optimal operating point for a given pump configuration. Such a model can be used to aid in the design of impedance pumps such as that of Rinderknecht, Hickerson & Gharib (2005).

† Present address: Keck Graduate Institute, 535 Watson Dr., Claremont, CA 91711, USA.

## 2. Methods

### 2.1. *Experimental setup*

The pump comprised an amber latex tube, 15 cm in length, 2 cm in diameter, and 0.08 cm in wall thickness, held horizontally. Its ends were fixed to rigid tubing that then connected to two reservoirs at each end of the test section. An additional rigid tube connected the reservoirs, creating a closed loop. The reservoirs had two purposes: to reduce the momentum of the flow exiting the pump such that the flow through the connecting loop is pressure driven, and to allow the system to be pressurized to different values with respect to the external pressure on the pliant section. Water, with a density of $10^3\,\mathrm{kg\,m^{-3}}$ and viscosity of $10^{-3}\,\mathrm{kg\,m^{-1}\,s^{-1}}$ was used as the working fluid. A secondary reservoir surrounded the elastic section to allow ultrasound imaging of the wall motion. A compression mechanism was built such that two mechanically linked pinchers could compress the elastic section from both sides.

### 2.2. *Measurement*

Measurement of the compliance of the elastic tube was performed by filling an isolated section of tubing with different volumes and measuring the change in transmural pressure (Stevanov, Baruthio & Eclancher 2000).

A normalized definition of the compliance, $C$, as a function of cross-sectional area, $A$, transmural pressure, $P$, and a cross-sectional area at rest of $A_0$ was used: $C = (\partial A/\partial P)/(A_0)$. The change in diameter was inferred by assuming uniform expansion of the tube based on the volume added. A constant value for the tube used was found to be $1.9 \times 10^{-2}\ \mathrm{kPa^{-1}}$.

Two diaphragm pressure transducers with a range of 34.5 kPa (5 PSI) and an accuracy of 0.1% were used to measure the pressure in time at both ends of the pliant section. An ultrasonic flow meter system was used to measure the dynamic flow rate at the exit. It has a range of $\pm 8.3 \times 10^{-4}\,\mathrm{m^3\,s^{-1}}$ ($50\ \mathrm{l\,min^{-1}}$), and a resolution of $4.2 \times 10^{-7}\,\mathrm{m^3\,s^{-1}}$ ($0.025\ \mathrm{l\,min^{-1}}$).

Ultrasound imaging was used for the measurement of wave speed on the surface of the tube. To accomplish this, the secondary reservoir was filled with water. An ultrasound probe was placed in the water to image axial slices of the tube. The edges of the axial slices were outlined and the cross-sectional width was measured along the length of the tube. By determining the positional shift of the cross-sectional width at a known frame rate, the wave speed was determined.

Filling of the secondary reservoir for ultrasound imaging had little effect on the frequency response curve provided the pressure across the tube wall was maintained. For experimental runs in which ultrasound images were not collected, the secondary reservoir was left empty. A description of the experimental setup and of the measurement systems can be found in more detail in the dissertation of Hickerson (2005).

## 3. Experimental wave behaviour

In the previous experiments of Hickerson *et al.* (2005), we observed distinct peaks in the frequency response of the net flow rate, as well as in the net pressure head across the pump. One such result can be seen in figure 4 using the parameters from table 2. These peaks motivated further experimentation to determine the wave behaviour responsible for creating such a response.

### 3.1. *Reservoir natural resonant frequency*

In an effort to separate the behaviour of the impedance pump from that of the flow loop including the reservoirs, the natural frequencies associated with the reservoirs

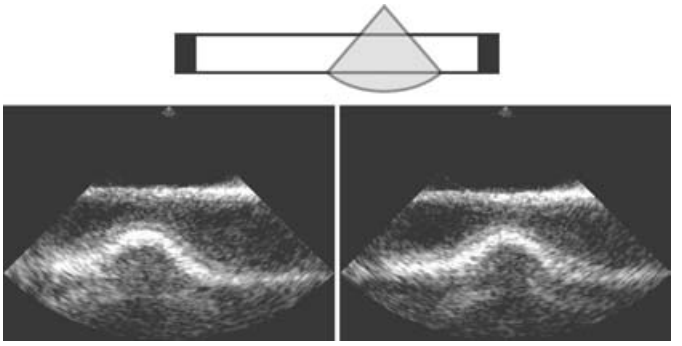

FIGURE 1. A wave travels to the right in these sample consecutive ultrasound images of a partial cross-section of the plaint tube. The position of the ultrasound probe is also shown in relation to the pliant tube.

and flow loop were measured with the pump removed. In its place was a short rigid tube of the same diameter. In this configuration, the system behaved as a simple harmonic oscillator with a resonant frequency far below the range of compression frequencies and measured flow frequencies.

### 3.2. *Wall motion*

Imaging of the sectional slices of the impedance pump showed wave propagation along the length of the tube and reflection at the end. It also showed that the tube did not expand in diameter but rather functioned as a pliant tube that can buckle. This is because the pressures created in the system are not high enough, given the compliance of the material used, to stretch the material beyond 1% of its resting diameter.

In the optimized case, one can observe that the frequency of compression matches the frequency with which the tube refills to its full diameter after the compression at the site of the compression. This corroborates prior experimental results that the impedance pump relies on resonance to build pressure and flow.

One example of ultrasound imaging can be seen in figure 1. A partial cross-section shows consecutive images of a wave travelling along the length of the tube.

### 3.3. *Pressure and flow relationship*

We examine the relationship between pressure and flow at one end of the elastic section for a fixed configuration during high positive net flow of $2.0 \times 10^{-5}$ m$^3$ s$^{-1}$ (1.2 l min$^{-1}$) with a net pressure head of 170 Pa (1.3 mm Hg) (3.4 Hz compression with 20 % duty cycle), low positive net flow of $4.2 \times 10^{-6}$ m$^3$ s$^{-1}$ (0.25 l min$^{-1}$) with a net pressure head of 80 Pa (0.6 mm Hg) (1.5 Hz compression with 20 % duty cycle), and high negative net flow of $6.7 \times 10^{-6}$ m$^3$ s$^{-1}$ (0.4 l min$^{-1}$) with a net pressure head of 93 Pa (0.7 mm Hg) (6.5 Hz compression with 20 % duty cycle) (figure 2). During the highest positive net flow, the pressure and flow appear to be locked in phase. This is a direct result of activating the resonant frequency of the system.

In the low flow and negative flow cases, the flow–pressure profile moves counter-clockwise in time. Just as the pressure drops, a flow begins to fill the low-pressure region from a higher-pressure region. The time at which this is observed at the two ends of the pliant tube is different in phase. Depending on the compression pattern, the position of the higher-pressure region varies. By modifying the frequency and duty cycle, a coordination between the two ends can achieved such that net unidirectional

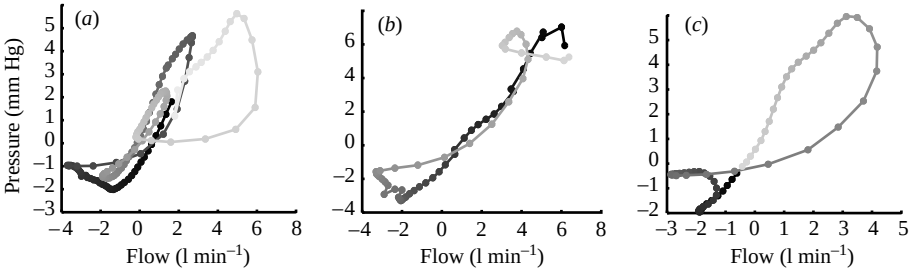


FIGURE 2. Transmural pressure versus flow rate measured at one end of elastic tube during (*a*) low flow (1.5 Hz), (*b*) high flow (3.4 Hz), and (*c*) negative flow (6.5 Hz) phase averaged over one pressure cycle. Points are separated at equal time steps moving forward from dark to light.

flow is sustained. The same phenomenon is observed when the flow is seeded with particles in an axial-slice ultrasound video. As the pressure decreases, the tube begins to collapse. When the travelling region of low pressure reaches the end it reflects off the impedance mismatch causing the tube to open. Fluid immediately begins to fill in from behind the wave front. Once the section has expanded to its resting diameter, it begins to exert pressure back into the fluid. It reaches a critical threshold when the pressure differential can no longer drive the flow in the same direction and the flow reverses.

### 3.4. *Transient response*

The resonant, pulsatile nature of the impedance pump led us to ask how long it takes to establish a net flow. A comparison between the moving average over one compression cycle of the flow in time was made between high positive net flow, low positive net flow, and high negative net flow for the same configuration as was used in determining the pressure–flow relationships. We find that for the high positive net flow case, an equilibrium is reached in 2 s corresponding to 7 compression cycles. For low flow and negative flow cases the time to reach equilibrium was 5 s, corresponding to as many as 30 compression cycles.

## 4. Wave pulse model

Approaches taken thus far to model the behaviour of an impedance pump can be divided into two broad categories: lumped models that build an analogy to known solvable systems such as electrical circuits and determine the response of those systems; and computational models that apply known fluid and structure laws to finite cells and determine the response computationally at small temporal and spatial steps. The computational results are more experimental in nature, whereas the lumped models make a prediction of the dominant mechanics.

We offer a third approach to modelling the impedance pump and predicting its behaviour. Experimental observation has shown us that pressure wave propagation and reflection in the fluid, made visible by the distortion of the surface of the pumping element, play an important role in the behaviour of the impedance pump. Starting from this point, we can create a wave model designed to mimic the wave properties of the impedance pump.

We begin with a line of fixed length that represents the length of the impedance pump along which a wave can travel: $-L \leqslant x \leqslant L$.

| Parameter | Symbol | Range |
|---|---|---|
| Compression location | $l$ | $-L < l < L$ |
| Width of compression | $w$ | $0 \leqslant w < L - \|l\|$ |
| Period | $T$ | |
| Duty cycle | $d$ | $0 \leqslant d \leqslant 1$ |
| Time step | $\mathrm{d}t$ | |
| Wave speed | $c$ | |
| Total simulation time | $\tau$ | |
| Amplitude decay constant | $r$ | $0 \leqslant r \leqslant 1/dt$ |
| Reflectance coefficient | $R$ | $0 \leqslant R \leqslant 1$ |
| Initial wave amplitude | $A_0$ | |
| Wave pulse width | $p$ | |
| Wave pulse shape | $P(x)$ | $P(x) = \exp(-2x^2/p)$ |

TABLE 1. Model parameters

Compression parameters can be chosen, including the location of the centre of compression, width, period and duty cycle. We use the assumption that a pair of pressure waves is emitted in opposite directions each time the tube is compressed. These waves are allowed to travel along the line, reflecting when they reach the ends of the line or the compression site if it is in the closed position. Additional configurable parameters of the model include the time step between calculations, wave speed, total simulation time, wave amplitude decay constant, reflectance coefficient, initial wave amplitude, wave pulse width, and wave pulse shape (table 1).

For each wave pair emitted, its start time, travel time, total distance travelled, directions, amplitudes, and positions are computed for small temporal steps. The start time for each pair is dependent on the compression period and is an integer multiple $n$ of the period $T$. The travel time is incremented by $\mathrm{d}t$ for each time step above the start time. It is equivalent to $t - nT$ for $t \geqslant nT$ and zero otherwise. The total distance travelled is the wave speed multiplied by the travel time, $c(t - nT)$ for $t \geqslant nT$, and zero otherwise. The direction parameter, dir, of each wave changes sign for each reflection encountered. It is positive for a wave moving in the positive $x$-direction and negative for a wave moving in the negative $x$-direction. The amplitude of each wave is based on an initial amplitude, chosen decay constant, and reflectance coefficient. Each wave is subjected to exponential decay in the form $A(t) = A(t - \mathrm{d}t)(1 - r\mathrm{d}t)$. And, for every reflection at the ends, the amplitude is decreased according to the reflectance coefficient such that $A(t) = RA(t - \mathrm{d}t)$. Finally, the positions are determined based on a fixed wave speed which in a real pump would be a result of the material properties, fluid properties, and transmural pressure. The position of the centre of the wave is therefore: $\mathrm{pos}(t) = \mathrm{pos}(t - \mathrm{d}t) + \mathrm{dir}\ c\mathrm{d}t$. In the event of a reflection at a site $x$, the position is adjusted according to $\mathrm{pos}(t) = -(\mathrm{pos}(t - \mathrm{d}t) + \mathrm{dir}\ c\mathrm{d}t) + 2x$. Each wave pulse is assumed to maintain a Gaussian shape defined by $P(x) = \exp(-2x^2/p)$, scaled by the wave amplitude, $A(t)$, and where $p$ is the width of the pulse. Each wave pulse shape is then reflected in the same manner as the wave position if it crosses a reflection site.

All of the waves are finally summed along the length of the line divided discretely into steps of length $\mathrm{d}L$ to form a spatial wave profile for each time step. The difference in the summed pressure wave amplitude at the ends of the line represents a value proportional to the pressure head of a similar pump. Once an equilibrium is reached a mean value of the amplitude difference can be taken for varying compression

| Parameter | Experiment | Simulation |
|---|---|---|
| Total time | 10 s | 10 s |
| Time step, d$t$ | NA | 10 msec |
| Wave speed, $c$ | 60 $\pm$10 m s$^{-1}$ | 50 m s$^{-1}$ |
| Length of tube, 2$L$ | 15 cm | 15 cm |
| Length step, d$L$ | NA | 0.01 cm |
| Compression location, $l$ | $-$5.1 cm | $-$5.1 cm |
| Width of compression, $w$ | 2.5 cm | 2.5 cm |
| Duty cycle, $d$ | 30 % | 30 % |
| Initial wave amplitude, $A_0$ | unknown | 3 |
| Waveform, $P(x)$ | unknown | 3 cm wide Gaussian |
| Amplitude decay constant, $r$ | unknown | 0.2 |
| Reflectance coefficient, $R$ | unknown | 0.5 |

TABLE 2. Parameters used for comparing experimental and simulated results.

frequencies. The model was implemented using C++ code with an approximate runtime of one second per average pressure-head datum point.

## 5. Model results

As a first test, the effects of modifying the model parameters on the pressure head as a function of compression frequency were compared to those known experimentally. We find that the net flow as a function of compression frequency shifts to higher frequencies with increased wave speed, similar to the experimental results of Hickerson *et al.* (2005). Additional results from the simulation show that the pulse width affects the amplitude but not the characteristic shape of the frequency response curve. Changes in the reflectance coefficient induce a similar behaviour. As the reflectance coefficient increases, so does the scale of the frequency response curve. As the reflectance coefficient goes to zero, no net difference is found across the pump.

The shapes of frequency response curves that the model produces vary greatly. Some may have broad humps while others have sharp peaks. Others still may be very chaotic in appearance. Curiously, the resulting curves are found not to be smooth or simple as one may expect from a linear, one-dimensional model.

A comparison can then be made between the experimental results and the simulation using parameters in the range known to be accurate for a specific experiment (table 2). Many of the parameters are easily applied from the experiments. The parameters that remain unknown are the amplitude of the pressure wave, the waveform including its shape and width, the amplitude decay constant, and the reflectance coefficient.

The initial wave amplitude, pulse width, and reflectance coefficient affect only the scale of the frequency response curve. If we use the simulated results to predict the shape but not the scale of the pressure head as a function of compression frequency, we can safely select those parameters arbitrarily. The shape of the waveform and the amplitude decay constant remain up to interpretation. The shape chosen was a simple Gaussian loosely based on the ultrasound images of the tube wall. The decay constant was also loosely based on the ultrasound images, then further refined to fit the experimental results to the simulated results as closely as possible.

The simulated results maintain most of the characteristics found in the experiments (figures 3, 4). There are distinct, sharp peaks at selected compression frequencies.

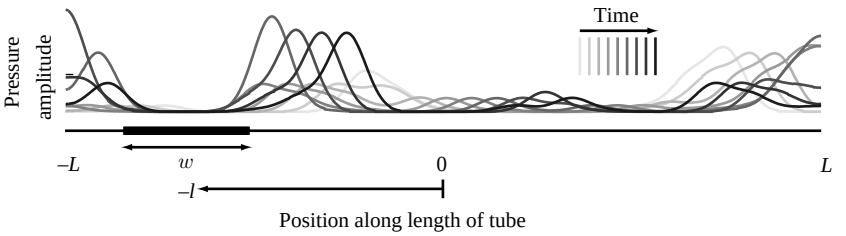


FIGURE 3. Simulation of pressure along the length of the pump for varying time.

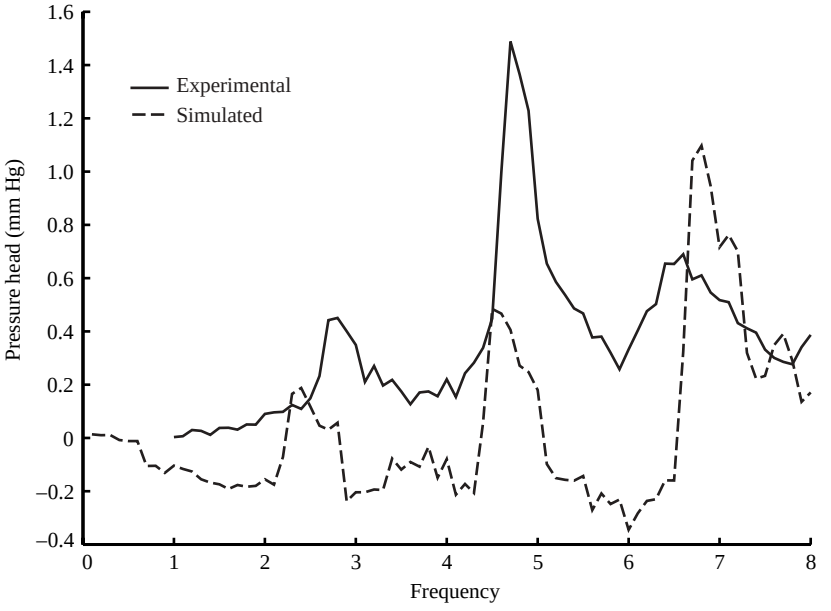


FIGURE 4. Simulation of net pressure head across the pump as a function of compression frequency compared with experimental results from Hickerson *et al.* (2005).

Those peaks lie at approximately the same locations. The scale of the simulated results remains arbitrary due to the random selection of values for the initial wave amplitude, pulse width, and reflectance coefficient which are responsible for the scale. Further refinement could be achieved from a saturation factor in which the amount of pressure added to the system would have a maximum based on current pressure at the compression site. This would lower the relative amplitude of peaks at increasing compression frequencies when it would be more likely for the compression to occur when the tube is already collapsed.

The resulting value of this simple wave model is in its prediction of both the shape of the pressure head as a function of time and the time-averaged pressure head as a function of compression frequency. The short time period of the calculation allows a quick estimate of a given pump's behaviour. Additionally, it may be used as an aid in a feedback system used to control such a valveless pump.

## REFERENCES

AUERBACH, D., MOEHRING, W. & MOSER, M. 2004 An analytical approach to the Liebau problem of valveless pumping. *Cardiovasc. Engng: Intl J.* **4** (2), 201–207.

Bertram, C., Raymond, C. & Pedley, T. 1991 Application of nonlinear dynamics concepts to the analysis of self-excited oscillations of a collapsible tube conveying a fluid. *J. Fluids Struct.* **5** (4), 391–426.

Borzi, A. & Propst, G. 2003 Numerical investigation of the Liebau phenomenon. *Z. Angew. Math. Phys.* **54** (6), 1050–1072.

Hickerson, A. I. 2005 An experimental analysis of the characteristic behaviors of an impedance pump. PhD thesis, California Institute of Technology.

Hickerson, A. I., Rinderknecht, D. & Gharib, M. 2005 Experimental study of the behavior of a valveless impedance pump. *Exps. Fluids* **38** (4), 543–540.

Jung, E. & Peskin, C. 2001 2-D Simulations of valveless pumping using immersed boundary methods. *SIAM J. Sci. Comput.* **23** (1), 19–45.

Kenner, T., Moser, M., Tanev, I. & Ono, K. 2000 The Liebau-effect or on the optimal use of energy for the circulation of blood. *Scripta Medica* **73** (1), 9–14.

Liebau, G. 1954 Über ein Ventilloses Pumpprinzip. *Naturwissenschaften* **41**, 327.

Mahrenholtz, V. O. 1963 Ein Beitrag zum Forderprinzip Periodisch Arbeitender, Ventilloser Pumpen/A contribution to the pumping principal of periodically acting valveless pumps. *Forsch. Auf Dem Gebiet Ing.* **29**, 47–56, 73–81.

Moser, M., Huang, J. W., Schwarz, G. S., Kenner, T. & Noordergraaf, A. 1998 Impedance defined flow: generalization of William Harvey's concept of the circulation – 370 years later. *Intl J. Cardiovasc. Med. Sci.* **1** (3/4), 205–211.

Ottesen, J. 2003 Valveless pumping in a fluid-filled closed elastic tube-system: one-dimensional theory with experimental validation. *J. Math. Biol.* **46** (4), 309–332.

Rinderknecht, D., Hickerson, A. I. & Gharib, M. 2005 A valveless micro impedance pump driven by electromagnetic actuation. *J. Micromech. Microengng* **15**, 861–866.

Stevanov, M., Baruthio, J. & Eclancher, B. 2000 Fabrication of elastomer arterial models with specified compliance. *J. Appl. Physiol.* **88**, 1291–1294.

Thomann, H. 1978 A simple pumping mechanism in a valveless tube. *Z. Angew. Math. Phys.* **29**, 169–177.